



This is a repository copy of *Low and ultra-low-cycle fatigue behavior of X52 piping steel based on theory of critical distances*.

White Rose Research Online URL for this paper:  
<http://eprints.whiterose.ac.uk/156265/>

Version: Accepted Version

---

**Article:**

Pereira, J.C.R., de Jesus, A.M.P., Xavier, J. et al. (3 more authors) (2020) Low and ultra-low-cycle fatigue behavior of X52 piping steel based on theory of critical distances. *International Journal of Fatigue*, 134. 105482. ISSN 0142-1123

<https://doi.org/10.1016/j.ijfatigue.2020.105482>

---

Article available under the terms of the CC-BY-NC-ND licence  
(<https://creativecommons.org/licenses/by-nc-nd/4.0/>).

**Reuse**

This article is distributed under the terms of the Creative Commons Attribution-NonCommercial-NoDerivs (CC BY-NC-ND) licence. This licence only allows you to download this work and share it with others as long as you credit the authors, but you can't change the article in any way or use it commercially. More information and the full terms of the licence here: <https://creativecommons.org/licenses/>

**Takedown**

If you consider content in White Rose Research Online to be in breach of UK law, please notify us by emailing [eprints@whiterose.ac.uk](mailto:eprints@whiterose.ac.uk) including the URL of the record and the reason for the withdrawal request.



[eprints@whiterose.ac.uk](mailto:eprints@whiterose.ac.uk)  
<https://eprints.whiterose.ac.uk/>

# LOW AND ULTRA-LOW-CYCLE FATIGUE BEHAVIOR OF X52 PIPING STEEL BASED ON THEORY OF CRITICAL DISTANCES

J.C.R. Pereira<sup>1</sup>, A.M.P. de Jesus<sup>1,2</sup>, J. Xavier<sup>3†</sup>, J.A.F.O. Correia<sup>1,4</sup>, L. Susmel<sup>5</sup>, A.A. Fernandes<sup>1,2</sup>

<sup>1</sup> *INEGI, Rua Dr. Roberto Frias, 4200-465 Porto, Portugal*

<sup>2</sup> *Faculty of Engineering, University of Porto, Rua Dr. Roberto Frias, 4200-465 Porto, Portugal*

<sup>3</sup> *UNIDEMI, Department of Mechanical and Industrial Engineering, Faculty of Sciences and Technology, Universidade NOVA de Lisboa, Caparica 2928-516, Portugal*

<sup>4</sup> *CONSTRUCT, Faculty of Engineering, University of Porto, Rua Dr. Roberto Frias, 4200-465 Porto, Portugal*

<sup>5</sup> *Department of Civil and Structural Engineering, The University of Sheffield, Mappin Street, Sheffield, S1 3JD, United Kingdom*

## **Abstract**

The cyclic failure observed in structural components such as pipelines subjected to extreme loading conditions highlights some limitations concerning the application of existing fatigue damage models. The evaluation and prediction of this type of failure in these steel components under large-scale plastic yielding associated with high levels of stress triaxiality are not sufficiently known nor explored. This fatigue domain is conventionally called ultra-low-cycle fatigue (ULCF) and damage features are representative of both low-cycle fatigue (LCF) and monotonic ductile fracture. Thus, in order to understand the ULCF damage mechanisms both monotonic and LCF tests are required to get representative bounding damage information to model the material damage behaviour under such extreme loading conditions. This paper aims at exploring the Theory of Critical Distances (TCD) in the LCF and ULCF fatigue regimes, including the application of the point, line and area methods. The application of the TCD theories has not been explored so far in the ULCF fatigue regimes, despite its promising results in the LCF and high-cycle fatigue. An experimental program was carried out on several specimens' geometries made of X52 piping steel. In detail, smooth plane specimens and notched plane specimens were cyclic loaded under tension/compression loading in order to obtain fatigue lives within the range of  $10^1$ - $10^4$  cycles. In addition, cyclic bending tests on notched plane specimens were also incorporated in this study. Finite element simulations of all small-scale tests were conducted allowing to derive

elastoplastic stress/strain fields along the potential crack paths. The numerical data were subjected to a post-processing in order to find characteristic lengths that can be treated as a fatigue property according to the TCD. A unified strain-life relation is proposed for the X52 piping steel together with a characteristic material length, consisting of a practical relation for pipeline strain-based design under extreme cyclic loading conditions.

## **Keywords**

*LCF, ULCF, Theory of Critical Distances, cyclic plasticity, piping steel.*

†Corresponding author.

E-mail: [jmc.xavier@fct.unl.pt](mailto:jmc.xavier@fct.unl.pt)

Tel.: +351 225091740; fax: +351 225081445

## 1. Introduction

Extreme loads applied to steel structures can lead to monotonic ductile fracture as well as to cyclic failure associated with large plastic deformations. Depending on the intensity of plastic deformation, cyclic failure may occur for a significantly reduced number of load cycles, which in some cases can be lower than 100 cycles. This is an extreme fatigue domain, the so-called Ultra-Low-Cycle Fatigue (ULCF) that is characterized by a mix of two competing damage mechanisms, since ULCF may be understood as a transition damage process between the monotonic ductile damage and the low-cycle fatigue (LCF) [1]. The contribution of each damage mechanism will depend on the number of cycles to failure and the influence of monotonic ductile damage mechanisms will increase as the number of cycles to failure approaches the unity.

Fatigue damage models for ULCF life assessment typically involve similar parameters as adopted in monotonic ductile models, for example, the accumulated equivalent plastic strain, the fracture strain, the stress triaxiality and the Lode angle parameters as reported by some authors [2]-[5]. Besides these parameters, the equivalent plastic strain range typically used in LCF also assumes an important role in ULCF modelling. Based on this set of parameters, the calibration of a ULCF model is dependent on a very specific experimental program involving both monotonic and ULCF tests coupled with finite element analyses. The numerical simulations are required to compute relevant parameters at locations where cracking is likely to occur. In what concerns the ULCF modelling, controlling parameters have been computed at nodes of the finite element model. However, this could be in contradiction with the Theory of Critical Distances (TCD), which suggests that the average values of the critical parameters around the specified potential critical location can be more representative of the damage process than the peak ones.

To establish correlations for both quasi-static and fatigue failure of smooth and notched specimens, the TCD has been originally used with specimens experiencing linear-elastic behaviour near the notch root. This theory was initially introduced by Neuber [6][7] and Peterson [8] and has been continuously developed and re-discovered by several researchers over extensive experimental campaigns and assuming linear-elastic local approaches [9][10]. Besides, Whitney and Nuismer [11] defined the characteristic length to calculate the brittle failures in notched details of composite materials, relating the smooth material strength to material toughness. This concept was reformulated and applied to the fatigue domain

by Tanaka [12] and Taylor [13]. Ductile metals under high levels of cyclic plasticity at the critical locations experience a reduction in the number of cycles to failure. This scenario is typically addressed under a strain-based approach framework, where the finite element simulations represent a crucial role in modelling the elastoplastic conditions at the damage process zone. Recent studies [14] have shown that TCD can be successfully used to predict fatigue failure under low-cycle fatigue conditions.

Having in mind the succeeded application of the TCD on LCF modelling, this work aims at addressing the performance of this theory on both LCF and ULCF domains. The experimental data derived from an extensive program carried out on small-scale specimens of X52 piping steel was used for this purpose. Besides using typical smooth specimen geometries, notched specimens were subjected to tension/compression cyclic tests. The experimental characterization of ULCF material is enhanced by using notched specimens since they tend to reduce instability problems typically observed at high plastic strain levels on smooth geometries. Additionally to the uniaxial cyclic tests, cyclic bending tests were also carried out on notched specimens, which included alternative stress/strain gradients on the results of the tests. Consequently, based on several geometries including notched and smooth specimens loaded at different loading scenarios, the TCD is understood as a robust data reduction approach, overcoming the challenges of the resulting non-uniform stress/strain fields. In the first part of the paper, the TCD will be reviewed covering the point, line and area methods to check the best appropriate TCD approaches for the X52 material. Furthermore, a unified strain-life relation will be sought for the X52 piping steel together with a characteristic material length, to result in a practical tool for pipeline strain-based design under extreme cyclic loading conditions.

## **2. Theory of critical distances (TDC)**

The failure prediction under high-cycle fatigue domain, particularly for notched details, could be too conservative if the linear-stress conditions at the notch root are considered, as reported by Neuber [6]. The actual stress considered for the fatigue damage evolution in the process zone is not as large as the peak value obtained using the classic continuum mechanics theory [6]. According to this author, the cyclic damage in the process zone is governed by the effective stress that results by averaging the linear-elastic stresses over a specified material characteristic length [15]. This assumption formulates the so-called Line Method (LM), where the effective stress is computed over the line, defined by the maximum

principal stress/strain distribution against a certain distance from the notch root, as evidenced by the Figure 1b.

This postulate can be extended to other fatigue regimes involving cyclic plastic deformations, such as the LCF. To estimate the fatigue lives under this specific fatigue domain a strain-based approach has been recommended aiming at increasing the predictive capability as originally proposed by Coffin [16] and Manson [17]. Therefore, the classical strain-life approach to address the fatigue life for any kind of notched components may be reformulated according to the TCD assumptions if the strain/stress field acting on the process fatigue location is known [18].

The application of the TCD can be done following different strategies, namely the Point Method (PM), Line Method (LM), Area Method (AM) and Volume Method (VM) [9]. The main goal of these methods is to achieve a given “characteristic length” which is used to describe an elastoplastic stress/strain state that is equivalent to the entire stress/strain field in the process damage zone. In detail, for the PM the effective stress/strain is computed directly from the stress/strain function, at a certain distance from the notch root, as proposed by Peterson [8] (see Figure 1a). Concerning the LM formulation, Neuber [6] assumed that the effective stress/strain results from the stress/strain distribution averaged over a line with a characteristic length, as illustrated in Figure 1b. For the implementation of the AM, the effective stress/strain is computed by averaging the stress/strain data over an area (e.g. semicircle with the geometrical centre coincident with the strain concentrator peak) as schematically represented in Figure 1c [13]. Similar arguments can be presented for the VM, which will not be explored in this research, therefore disregarded from this analysis. To apply the PM, LM and AM the critical distances are expressed as  $L_{PM} = L/2$ ,  $L_{LM} = 2L$  and  $L_{AM} = L$ , respectively, where  $L$  is the material characteristic length, which does not depend on the specific features of the stress/strain field [19]. Regarding the strain-based approach, and adopting the nomenclature of Figure 1, the LM, PM, and AM can be expressed, respectively, as follows [19]:

$$\varepsilon_{eff} = \varepsilon_1 \left( \theta = 0, r = \frac{L}{2} \right) = \varepsilon_a \quad (1)$$

$$\varepsilon_{eff} = \frac{1}{2L} \int_0^{2L} \varepsilon_1(\theta = 0, r) dr = \varepsilon_a \quad (2)$$

$$\varepsilon_{eff} = \frac{1}{1.1} \frac{1}{\pi L^2} \int_0^{\pi/2} \int_0^L \varepsilon_1(\theta, r) \cdot r \cdot dr \cdot d\theta \cong \varepsilon_a, \quad (3)$$

where  $\varepsilon_a$  is the strain amplitude. The TCD has been demonstrated to be successful for LCF conditions [14]. Nevertheless, the application of the TCD under ULCF conditions has never been demonstrated before. Therefore, this paper will assess the TCD in the forms of PM, LM, and AM to conditions of LCF and ULCF and results will be compared with those resulting from the application of the peak values of the influent damage variables evaluated at the notch root, called in this paper as critical node approach.

### 3. Critical node approach

An extensive experimental program was carried out aiming at investigating the performance of the TCD on fatigue life estimation under large plastic strain amplitudes. Specimens were cut along the longitudinal direction of pipes made of X52 steel grade with the following dimensions: outside diameter of 168 mm and the wall thickness of 4.78 mm. As previously referred to, smooth and notched plane specimens were subjected to cyclic tests to result in fatigue lives under both LCF and ULCF domain ( $10^0$ - $10^4$  cycles). Fatigue tests were carried out on a servo-hydraulic INSTRON® 8801 testing machine. The tests were performed under locally controlled displacements using an INSTRON® 2620-602 clip gauge, with limit displacements of  $\pm 2.5$  mm. Constant strain or constant relative displacement rates, respectively  $d\varepsilon/dt=0.8$  or  $d\delta/dt=0.8$ , were adopted in the cyclic tests. The frequency of the cyclic tests was set as a function of the strain or relative displacement. This resulted in controlled uniform strains for smooth specimens. For notched specimens, the strain-field was not uniform; therefore, the locally controlled displacements were used as input of the finite element models. Accordingly, the strain range (smooth specimens) and relative displacement range (notched specimens) were given by:

$$\Delta\varepsilon, \Delta\delta = \frac{\Delta l}{L_0} \times 100 \quad (4)$$

The strain or relative displacement ratios used for each type of specimen geometries are summarized in Table 1. The geometries of these specimens are illustrated in Figures 2 and 3. It should be noted that the ductility of the specimens is affected by the notch configuration that in turn provide different levels of fracture strain and stress triaxiality levels. These monotonic parameters are helpful to calibrate some fatigue damage models (ex. Xue model) [1]. The specimens were of plane dog-bone type, with some series showing different notches (circular and oval central holes and double side circular notches).

Additional experimental details regarding the ranges of strain/relative displacements and testing frequencies considered for the fatigue tests can be found elsewhere [20].

The cyclic/elastoplastic properties of the X52 piping steel were already presented in a previous study carried out by Pereira *et al.* [21]. Concerning the numerical simulation of the cyclic tests, a plasticity model based on the second invariant of the stress tensor (Von Mises yield theory) with nonlinear kinematic hardening (Chaboche model) was used [22]. The cyclic properties expressed in terms of the mathematical relation proposed by Ramberg and Osgood,  $K'$  and  $n'$ , [23] and the parameters used to define the plasticity model of the X52 piping steel are respectively presented in Table 2. A 3D geometry with 8-noded isoparametric solid elements with reduced integration, C3D8R, available on commercial code ABAQUS 6.12<sup>®</sup> was built to model de plane notched specimens. Taking into account the symmetry boundary conditions, whenever possible, only 1/8 of the geometry was modelled. The displacements of nodes laying at the symmetry planes were restrained along the direction normal to that symmetry planes. The refined mesh, with a minimum element size of 0.17 mm was deemed suitable for the proposed analyses to reduce the mesh size effect on the computation of stress and strain fields.

Additional details about this study, namely the fatigue testing and the calibration of the plasticity model can be found elsewhere [21]. Before the application of the TCD, a critical node approach supported by the strain-life Morrow's relation [24] is followed. Morrow's equation results from the superposition of the elastic strain-life and plastic strain-life relations, defined respectively by Basquin [25] and Coffin-Manson [16],[17] equations, as follows:

$$\frac{\Delta \varepsilon}{2} = \frac{\Delta \varepsilon^E}{2} + \frac{\Delta \varepsilon^P}{2} = \frac{\sigma_f'}{E} (2N_i)^b + \varepsilon_f' (2N_i)^c. \quad (5)$$

In order to introduce the multiaxial effects caused by the notch presence, the equivalent strain definition proposed by the ASME code [26] was used:

$$\Delta \varepsilon_{eq}^p = \frac{\sqrt{2}}{3} \sqrt{(\Delta p_{11} - \Delta p_{22})^2 + (\Delta p_{22} - \Delta p_{33})^2 + (\Delta p_{33} - \Delta p_{11})^2 + \frac{3}{2}(\Delta p_{12}^2 + \Delta p_{23}^2 + \Delta p_{31}^2)} \quad (6)$$

where  $\Delta p_{ij}$  denotes the plastic strain component variation between two consecutive load reversal points.

This formulation is proposed originally in the ASME code for the computation of the plastic component of equivalent strain range but, in this case, it was also extended to derive the equivalent elastic strain range.

The parameters of Morrow relation ( $\sigma'_f$ : fatigue strength coefficient;  $b$ : fatigue strength exponent;  $\varepsilon'_f$ : fatigue ductility coefficient;  $c$ : fatigue ductility exponent) were computed correlating the elastic and plastic equivalent strain ranges with the number of cycles until crack initiation, for all tested smooth and notched specimens and respective values are summarized in Table 3. As mentioned above, the fatigue life was investigated until crack initiation. Therefore, a criterion to identify the number of cycles to crack initiation was suggested, by plotting the maximum load values along with the number of cycles, as shown in Figure 4. The fatigue crack initiation was assumed to occur when the maximum load values start to deviate from the stable trend, which corresponds to the macroscopic fatigue crack propagation.

Figure 5 illustrates the strain-life curve correlating the experimental data points. Some scatter is found between notched and smooth specimen series, mainly in the ULCF domain. The notch presence promotes local strain concentration and consequent strain gradients in the plastic strain field. The use of an equivalent strain range definition was not enough to overcome this modelling limitation. Using the parameters of Morrow's relation and the equivalent plastic strain ranges derived from finite element simulations of each specimen simulation, fatigue life estimations were computed and compared with the experimental results, as can be observed in Figure 6, including both LCF and ULCF regimes. Accuracy bands were added to the graphs with a twice (2x) and half (0.5x) lives criteria being used for the LCF domain and a progressive accuracy band used for ULCF, reducing its width (increasing accuracy) from twice/half-lives in the LCF to 1.33x/0.75x of experimental fatigue lives at  $N_f=1$  cycle. Reasonable fatigue life estimations can be observed for notched specimens under ULCF and LCF regimes. Nevertheless, the Morrow's relation using a critical node approach does not provide excellent predictions for smooth specimens in both fatigue domains addressed in this study.

#### **4. Calibration of the TCD methods on LCF and ULCF life prediction**

In this section, the TCD is applied together with the Morrow's relation. The PM, LM and AM are applied to compute the elastic and plastic effective strains that will be correlated with the number of reversals until the crack initiation. These correlations provide updated Morrow parameters that will be considered to estimate the fatigue life of the specimens covered in this work. The total and plastic strain fields were computed and mapped for each specimen. The resulting strain maps allowed the understanding of the strain gradients around the hypothetical crack initiation and propagation path. The main crack propagation direction was assumed along the specimen width/transverse to the loading direction, as

supported by the analysis of Figure 7. The analysis of the fracture surface aiming to identify the characteristic features of a fatigue failure under large plastic strain conditions. Therefore the crack initiation (1), the crack propagation processes characterized by the beach-marks (2) and the final plastic failure (3) are observed. Under the ULCF domain the plastic strains are intense, thus the beach-marks are more noticeable in the fracture surfaces. These features mark the progress of the crack at various stages of the cyclic loading.

The simulation of the cyclic tests of smooth specimens accounted for lateral instabilities that may arise from high compressive stress/strains, therefore the location of crack initiation could be variable despite occurring at the specimens' surface [21]. Thus, the crack propagation direction was set from the node with the higher equivalent total strain (critical node). The evolution of equivalent total strain along the crack propagation direction is represented in Figure 8. Combining the TCD formulations in Eqs. (1), (2) and (3) and the hypothetical crack path orientation at the crack propagation plane, the effective equivalent total and plastic strains were computed for each specimen. Regarding PM, the effective strain components were directly obtained from the evolution of the equivalent total and plastic strains along the crack path while for the LM the effective total and plastic strains were achieved by means of numerical integration of a polynomial function fitted to the equivalent total and plastic strain along the crack path. Moreover, concerning the AM, the effective strain was calculated by averaging the strain data over a semicircular area with the geometrical centre coincident with the strain concentrator/critical node, as represented in Figure 9.

The methodology for the assessment of the critical distance  $L$  is described below. On effect, to estimate the critical distance  $L$  to be applied with the PM, LM and AM a try and error (iterative) method was proposed aiming at maximizing the correlation between the experimental data and the Morrow's relation prediction. In detail, the PM, LM, and AM were applied covering several critical distances ( $L$  values), which resulted in several fatigue life estimations using the Morrow's relation. The correlation between the experimental number of cycles and numerical fatigue life predictions was measured based on the coefficient of determination,  $R^2$ , of the least-squares regression algorithm. The  $R^2$  values were plotted against the distance  $L$ , as shown in Figure 10. A polynomial function with degree six was used to fit the data. The proposed method for identification of  $L$  corresponds to an inverse approach. The proposed critical distances should maximize the coefficient of determination between the Morrow's relation and the experimental data from distinct sources/notched details. Table 4 summarizes the maximum  $R^2$  and

associated critical distances ( $L$ ) concerning the different TCD approaches. The resulting critical distances (characteristic lengths) depended on the TCD approach. The PM approach was the one that resulted in the highest  $R^2$  with a characteristic length,  $L=0.27$ . Table 5 presents the parameters of Morrow's equation resulted in the maximum coefficient of determination and characteristic lengths shown in Figure 10 and Table 4.

The plot of the total strain-life data using the critical distance identified from the methodology previously described and the PM (best prediction method) is shown in Figure 11. As it can be seen, the use of TCD/PM on fatigue life correlation of both smooth and notched specimens of X52 steel grade based on Morrow's relation, yields a clear improvement comparing to results obtained with the critical node approach (see Figure 5). The analysis of this figure exhibits significant enhancements regarding the ULCF results correlation, mainly for the smooth specimens data. An alternative representation that allows the assessment of the accuracy of the TCD/PM is presented in Figures 12 and 13 in the form of experimental data *versus* predicted results, the latter ones obtained with the Morrow's constants presented in Table 5 and characteristic length presented in Table 4. A very good agreement is verified even taking into account the progressive accuracy band for the ULCF, as could be realized by comparison with the results of Figure 6 corresponding to the critical node method. Also, the accuracy bands could be further narrowed. For the LCF regime, the double and half-life criterion can be replaced by a  $1.75\times$  and  $0.57\times$  criterion. For the ULCF domain, the progressive accuracy condition can be adjusted, reducing the accuracy band from LCF to  $1.25\times/0.8\times$  of experimental fatigue life in the ULCF ( $N_i=1$  cycle), and still encompassing all experimental data.

Also, the root mean square error (RMSE) (Eq. (7)) and the mean relative error (MRE) (Eq. (8)) of the number of cycles computed from critical node and PM/TCD approach were estimated and presented in Table 7, according to Barbosa et al. [27,28,29]. The consistency of the results obtained confirms the improvement of the fatigue predictions using the PM/TCD method regarding the critical node approach. It should be noted that the major improvements are observed for the LCF regime since the elastoplastic strain field gradient should be more noticeable in this fatigue regime rather than in the ULCF where generalized plasticity is verified. Nevertheless, it is demonstrated that the PM/TCD could be used for LCF data correlation and extrapolation to the ULCF can be properly admitted.

$$RMSE = \sqrt{\frac{1}{n} \sum_{i=1}^n (N_{num(i)} - N_{exp(i)})^2} \quad (7)$$

$$MRE = \frac{1}{n} \sum_{i=1}^n \frac{|N_{num(i)} - N_{exp(i)}|}{N_{exp(i)}} \quad (8)$$

## 5. Application of TCD/PM to the fatigue prediction of cyclic bending testing results

As previously presented in this paper, data of tensile/compressive cyclic tests using plane (smooth and notched specimens) was used to investigate the performance of TCD approaches to correlate the fatigue lives in the ULCF and LCF regimes. The previous analysis with the PM, LM and AM resulted in the determination of different characteristic lengths associated with X52 piping steel. However, the PM revealed to be superior in the correlation of the experimental data and this version of the TCD will be applied in this section with the respective Morrow's equation in the fatigue life predictions for extra cyclic bending tests performed in the ULCF regime.

In addition to the tensile/compressive cyclic tests, bending cyclic tests were also performed on notched plane specimens, which geometry is shown in Figure 14. As reported by Tateishi [4], Ohata [30] and Nip [31], cyclic bending tests can be considered as an alternative procedure to investigate the cyclic/damage behaviour of the materials under large plastic strain conditions. This observation is supported by the fact that this testing configuration overcomes the specimen instabilities that may occur under compressive stages of tension/compression tests, leading consequently to a reduced number of cycles until crack initiation. The experimental program of the bending cyclic tests was carried out on an INSTRON® 8801 servo-hydraulic test machine, at room temperature, under displacement control,  $R_d = 0$  and using a load cell rated to 5kN. A grip system was designed to induce an eccentric compressive load, as shown schematically in Figure 15a. The experimental set-up of bending cyclic tests is represented in Figure 15b. The applied displacement range,  $\Delta d$ , and the number of cycles to crack initiation,  $N_i$ , are summarized in Table 6. In order to apply the formulation inherent to TCD/PM, numerical FEM elastoplastic simulations of the bending cyclic tests were conducted aiming at reproducing the elastoplastic strain conditions where the fatigue cracking is expected to occur. The same plastic model with kinematic hardening considered for the numerical analysis of the tension/compression tests was used on the simulation of cyclic bending tests. In detail, the numerical P-d curve is correlated with the experimental response in Figure 16a, illustrating the good performance of the numerical model on the reproduction of cyclic loading.

Additional correlations between numerical and experimental evidences can be found elsewhere [32]. The equivalent plastic strain field on the central section of the specimens was evaluated in order to assess the location where the fatigue crack is supposed to occur, as can be observed in Figure 16b. This procedure allowed the computation of both elastic and plastic effective strains, for the characteristic length previously derived for the X52 piping steel (PM method) (see Table 4). The number of cycles to crack initiation of bending cyclic tests were computed and the comparison between the numerical and experimental results are plotted in Figure 17. The application of TCD/PM together with the Morrow's model resulted in the very good prediction of the number of cycles to crack initiation of the tested specimens, inside accuracy bands proposed for ULCF.

## 6. Conclusions

The performance of the TCD on ULCF and LCF life prediction was investigated in this paper considering a multiaxial strain-based method. The total, plastic and elastic strain components were computed following a multiaxial strain approach definition, according to Morrow's relation and it was able to reproduce the strain-life behaviour of the X52 piping steel, covering both fatigue regimes investigated in this work. Although generally accepted that both fatigue regimes may exhibit distinct damage mechanisms, the Morrow relation was still able to correlate the experimental data in both regimes. The elastoplastic TCD applied in the form of PM, LM and AM were able to predict the fatigue failure under high plastic strain levels with more accuracy than the typical approach based on the critical node. However, the different approaches for the TCD resulted in distinct characteristic lengths. In general, successful results for smooth and notched specimens were obtained independently of the adopted methodology. However, the PM revealed the most accurate TCD approach. The critical distances were found to be different depending on the TCD approach, but the PM was considered the most representative one due to the higher degree of correlation achieved with the experimental data. Also, it allows an easier application than LM or AM in terms of the required post-processing. The better accuracy of the PM/TCD was consistently demonstrated using different error criteria, the errors being smaller in the LCF than in ULCF regimes. It was demonstrated that the PM/TCD could be identified for the LCF regime and successfully used for ULCF predictions.

Alternative loading conditions were investigated, in particular covering bending loading of notched specimens. Using the TCD/PM and Morrow's based approach it was possible to get a very good

prediction of the fatigue lives for these tests, confirming the validity of the TCD for other stress/strain gradients.

As a future research activity, it is proposed the investigation of the sensitivity of the TCD under different levels of stress triaxialities and Lode angle parameters. In fact, the influence of these stress parameters has been investigated under monotonic ductile fracture, but more recent studies have shown that these parameters can assume an important role under ULCF failure [5]. The TCD also needs to be addressed simultaneously for distinct fatigue regimes (very-low, low- and high-cycle fatigue) in order to check if the critical distance parameter allows any generalization or if improvements of the TCD are required.

## Acknowledgements

The authors acknowledge the FCT - Portuguese Foundation for Science and Technology, for their financial support through the SFRH/626/BD/80091/2011 Grant and the projects UID/EMS/00667/2019. The European Commission is also acknowledged through the Research Fund for Coal and Steel that is funding the ULCF project. Additionally, the authors gratefully acknowledge the funding of SciTech - Science and Technology for Competitive and Sustainable Industries, R&D project cofinanced by Programa Operacional Regional do Norte (“NORTE2020”), through Fundo Europeu de Desenvolvimento Regional (FEDER). Finally, the authors would also like to acknowledge to the postdoctoral grant SFRH/BPD/107825/2015 (Portuguese Science Foundation, FCT/MCTES), and to the research unit CONSTRUCT of the University of Porto (POCI-01-0145-FEDER-007457, UID/ECI/04708/2019, FEDER, and FCT/MCTES).

## References

- [1] Pereira JCR, de Jesus AMP, Xavier J, Fernandes AA. Ultra low-cycle fatigue behavior of a structural steel. *Eng Struct* 2014;60:214 – 22. <https://doi.org/10.1016/j.engstruct.2013.12.039>
- [2] Xue L. A unified expression for low cycle fatigue and extremely low-cycle fatigue and its implication for monotonic loading. *Int J Fatigue* 2008;30:1691–98. <https://doi.org/10.1016/j.ijfatigue.2008.03.004>
- [3] Kanvinde AM, Deierlein GG. Cyclic void growth model to assess ductile fracture initiation in structural steels due to ultra-low cycle fatigue”, *J Eng Mech–ASCE* 2007;133:701–12. [https://doi.org/10.1061/\(ASCE\)0733-9399\(2007\)133:6\(701\)](https://doi.org/10.1061/(ASCE)0733-9399(2007)133:6(701))
- [4] Tateishi K, Hanji T. Low cycle fatigue strength of butt-welded steel joint by means of new testing system with image technique. *Int J Fatigue* 2004;26:1349–56. <https://doi.org/10.1016/j.ijfatigue.2004.03.016>
- [5] Pereira JCR, de Jesus AMP, Fernandes AA. A new ultra-low cycle fatigue model applied to the X60 piping steel. *Int J Fatigue* 2016;93:201–13. <https://doi.org/10.1016/j.ijfatigue.2016.08.017>
- [6] Neuber H. *Theory of notch stresses: principles for exact calculation of strength with reference to structural form and material*. 2nd ed. Springer-Verlag: Berlin; 1958.
- [7] Neuber H. Theory of stress concentration for shear-strained prismatical bodies with arbitrary nonlinear stress-strain law. *ASME J Appl Mech* 1961;28:544–50. <https://doi.org/10.1115/1.3641780>
- [8] Peterson RE. Notch Sensitivity. In: Sines G., Waisman, JL, editors. *Metal Fatigue*, McGraw Hill, New York; 1959, p. 293–306.

- [9] Taylor D. The theory of critical distances: a new perspective in fracture mechanics, Oxford: Elsevier. 2007.
- [10] Susmel L, Taylor D. Fatigue design in the presence of stress concentrations. *J Strain Anal Eng* 2003;38:443–52. <https://doi.org/10.1243/03093240360713496>
- [11] Whitney JM, Nuismer RJ. Stress fracture criteria for laminated composites containing stress concentrations,” *J Compos Mater* 1974;8:253–65.
- [12] Tanaka K. Engineering formulae for fatigue strength reduction due to crack-like notches. *Int J Fracture* 1983;22:R39–R45. <https://doi.org/10.1007/BF00942722>
- [13] Taylor D. Geometrical effects in fatigue: a unifying theoretical model. *Int J Fatigue* 1999;21:413–20. [https://doi.org/10.1016/S0142-1123\(99\)00007-9](https://doi.org/10.1016/S0142-1123(99)00007-9)
- [14] Susmel L, Taylor D. An elasto-plastic reformulation of the theory of critical distances to estimate lifetime of notched components failing in the low/medium-cycle fatigue regime. *J Eng Mater Technol* 2010;132: 210021–28. <https://doi.org/10.1115/1.4000667>
- [15] Susmel L, Taylor D. On the use of the Theory of Critical Distances to predict static failures in ductile metallic materials containing different geometrical features. *Eng Fract Mech* 2008;75:4410–21. <https://doi.org/10.1016/j.engfracmech.2008.04.018>
- [16] Coffin LF. A study of the effects of cyclic thermal stresses on a ductile metal. *Trans ASME* 1954;76:931–50.
- [17] Manson SS. Behaviour of materials under conditions of thermal stress. National Advisory Committee for Aeronautics, NACA TN-2933; 1954.
- [18] Susmel L, Taylor D. Estimating lifetime of notched components subjected to variable amplitude fatigue loading according to the elasto-plastic Theory of Critical Distances. *J Eng Mater Technol* 2015;137:11008–23. <https://doi.org/10.1115/1.4028927>
- [19] Susmel L. The theory of critical distances: a review of its applications in fatigue. *Eng Fract Mech* 2008;75:1706–24. <https://doi.org/10.1016/j.engfracmech.2006.12.004>
- [20] Pereira JCR, “Characterization of X52, X60 and X65 steel grades under monotonic and Ultra-low-cycle fatigue loading”, Phd Thesys 2016, Faculty of Engineering of the University of Porto.

- [21] Pereira JCR, de Jesus AMP, Fernandes AA, Varelis. Monotonic, Low-Cycle Fatigue, and Ultralow-Cycle Fatigue Behaviors of the X52, X60, and X65 Piping Steel Grades. *Journal of Pressure Vessel Technology* 2015;138:31403–10. <https://doi.org/10.1115/1.4032277>
- [22] Khan AS, Huang S. *Continuum Theory of Plasticity*. 1st ed. Wiley: New York; 1995.
- [23] Ramberg W, Osgood WR. Description of the stress-strain curves by three parameters. National Advisory Committee for Aeronautics; Washington, DC, NACA Technical Note 902; 1943.
- [24] Morrow JD. Cyclic plastic strain energy and fatigue of metals. In: Lazan B, editor. *International Friction, Damping and Cyclic Plasticity*, ASTM, STP 1965;378:45–87.
- [25] Basquin OH. The exponential law of endurance tests. *Proceedings of the American Society for Testing and Materials*, 1910;10:625–30.
- [26] ASME. *ASME Boiler and Pressure Vessel Code*. ASME, New York; 2004.
- [27] Barbosa JF, Carlos Silverio Freire Júnior R, Correia JAFO, De Jesus AMP, Calçada RAB. Analysis of the fatigue life estimators of the materials using small samples. *J Strain Anal Eng Des* 2018;53(8):699-710.
- [28] Barbosa JF, Correia JAFO, Montenegro PA, Júnior RCSF, Lesiuk G, De Jesus AMP, et al. A comparison between S-N logistic and kohout-věchet formulations applied to the fatigue data of old metallic bridges materials. *Frat Integrita Strutr* 2019;13(48):400-410.
- [29] Barbosa JF, Correia JAFO, Freire Júnior RCS, Zhu S-, De Jesus AMP. Probabilistic S-N fields based on statistical distributions applied to metallic and composite materials: State of the art. *Adv Mech Eng* 2019;11(8):1-22.
- [30] Ohata M, Toyoda M. Damage concept for evaluating ductile cracking of steel structure subjected to large-scale cyclic straining. *Sci Technol Adv Mat* 2004;5:241–49.  
<https://doi.org/10.1016/j.stam.2003.10.007>
- [31] Nip KH, Gardner L, Davies CM, Elghazouli DAY. Extremely low cycle fatigue tests on structural carbon steel and stainless steel. *J Constr Steel Res* 2008;66:96–110.  
<https://doi.org/10.1016/j.jcsr.2009.08.004>

[32] Pereira JCR, de Jesus AMP, Xavier J, Fernandes AA. ULCF assessment of X52 piping steel by means of cyclic bending tests. *J Constr Steel Res* 2017;138:663–74.

<https://doi.org/10.1016/j.jcsr.2017.08.020>

## List of Tables

Table 1. Strain ratios, $R_\epsilon$ , or relative displacement ratios, $R_\delta$ , used in the cyclic tests.....	2
Table 2. Cyclic properties and Chaboche parameters of the X52 piping steel. ....	2
Table 3. Parameters of Morrow's relation for the X52 piping steel obtained with critical node approach. ....	2
Table 4. Critical distances and respective determination coefficients associated with distinct TCD methods.....	2
Table 5. Parameters of Morrow's relation of X52 piping steel obtained with PM, LM and AM with characteristic lengths of Table 4. ....	2
Table 6. Experimental results of notched plane specimens of cyclic bending tests (U_BNP). ....	2
Table 7. Comparison of RMSE and MRE of life predictions obtained with critical node and PM/TCD approaches considering the complete dataset, ULCF and LCF.....	3

**Table 1.** Strain ratios,  $R_\epsilon$ , or relative displacement ratios,  $R_\delta$ , used in the cyclic tests.

	LCF tests	ULCF tests
Smooth specimens	$R_\epsilon = 0, R_\epsilon = -1$	$R_\epsilon = 0$
Notched specimens	$R_\delta = -1$	$R_\delta = 0, R_\delta = -1$

**Table 2.** Cyclic properties and Chaboche parameters of the X52 piping steel.

Cyclic properties	$K'$ [MPa]		$n'$	
		951.9		0.1538
Chaboche parameters	$\sigma_{y/0.2\%}$ [MPa]	$C^1$ [MPa]	$C^2$ [MPa]	$C^3$ [MPa]
	400	13000	150	700
	$\gamma^1$	$\gamma^2$	$\gamma^3$	
	150	20	1	

**Table 3.** Parameters of Morrow's relation for the X52 piping steel obtained with critical node approach.

Piping Steel	$\sigma'_f$ [MPa]	$b$	$\epsilon'_f$	$c$
X52	810.34	-0.0901	1.1316	-0.7117

**Table 4.** Critical distances and respective determination coefficients associated with distinct TCD methods.

Piping steel	$R^2$	L [mm]	TCD method
X52	0.916	0.27	PM
	0.912	0.12	LM
	0.908	0.25	AM

**Table 5.** Parameters of Morrow's relation of X52 piping steel obtained with PM, LM and AM with characteristic lengths of Table 4.

Piping steel	$\sigma'_f$	$b$	$\epsilon'_f$	$c$	TCD method
X52	756.21	-0.0781	0.8784	-0.6591	PM
	711.58	-0.0728	0.6458	-0.6406	LM
	746.56	-0.0745	0.9986	-0.6643	AM

**Table 6.** Experimental results of notched plane specimens of cyclic bending tests (U\_BNP).

Specimens	$\Delta d$ [mm]	$N_i$ [cycles]
U_BNP_1	100	4
U_BNP_2	150	2
U_BNP_3	70	10
U_BNP_4	70	7
U_BNP_5	70	12
U_BNP_6	50	14
U_BNP_7	50	13
U_BNP_8	50	14
U_BNP_9	35	20
U_BNP_10	100	5
U_BNP_11	20	60
U_BNP_12	20	60
U_BNP_13	15	93
U_BNP_14	15	99
U_BNP_15	15	61

**Table 7.** Comparison of RMSE and MRE of life predictions obtained with critical node and PM/TCD approaches considering the complete dataset, ULCF and LCF.

	RMSE		MRE	
	Critical Node	PM/TCD	Critical Node	PM/TCD
All data	597	451	24%	21%
ULCF	14	12	24%	21%
LCF	941	711	26%	22%

## List of Figures

Fig 1. Illustration of the TCD proposed to compute the effective strain: a) PM; b) LM and c) AM. .....	2
Fig 2. Smooth plane specimen geometry of X52 piping steel (X52_SP).....	2
Fig 3. Notched plane specimens' geometries of X52 piping steel: a) central oval hole (X52_OH); b) central circular hole (X52_CH); c) double side notched (X52_SN).....	3
Fig 4. Criterion to assess the fatigue crack initiation (X52_U0_SP_12). ....	3
Fig 5. Total strain-life data of the X52 piping steel and correlation using Morrow relation with critical node approach.....	3
Fig 6. Comparison of experimental data and Morrow's predictions based on critical node approach predictions, for the X52 piping steel. ....	4
Fig 7. Fracture surface of smooth plane specimens of X52 piping steel, tested under ULCF domain ( $\Delta\epsilon=5\%$ ).....	4
Fig 8. Equivalent total strain distribution along crack propagation direction of notched specimen (X52-U-1_OH_01).....	4
Fig 9. a) Illustration of the relevant effective equivalent total strain computation for the TCD using AM method (Z – loading direction); b) circular region considered to estimate effective equivalent total strain. ....	5
Fig 10. Determination coefficient $R^2$ as function of critical distance, $L$ . ....	5
Fig 11. Correlation of the strain-life data obtained with the effective equivalent total strain computed using the TCD/PM ( $L=0.27$ mm).....	5
Fig 12. Comparison of experimental data and Morrow's predictions based on point method approach predictions, for the X52 piping steel.....	6
Fig 13. Comparison of experimental data and Morrow plus PM method for X52 piping steel under LCF (a) and ULCF (b) domains. ....	6
Fig 14. The geometry of plane notched specimen of X52 piping steel submitted to cyclic bending conditions (X52_BNP).....	6
Fig 15. a) Loading conditions of the cyclic bending tests; b) grip system mounted in the test machine.....	7
Fig 16. a) Numerical load-displacement curves correlated with experimental data (X52_U_BNP_01); b) equivalent total strain field indicates the location for the crack initiation (X52_U_BNP_13).....	7
Fig 17. Prediction of the fatigue lives for the notched bending specimens made of X52 piping steel (X52_BNP) using the TCD/PM with Morrow's equation. ....	7

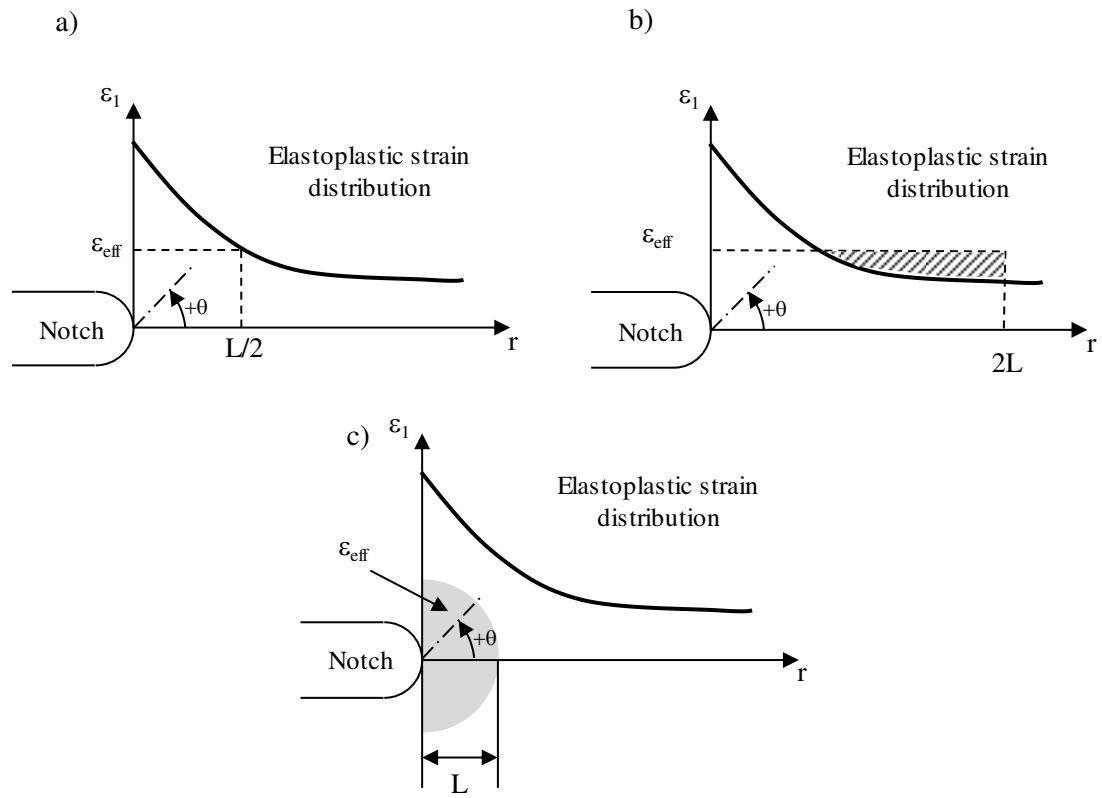


**Fig 1.** Illustration of the TCD proposed to compute the effective strain: a) PM; b) LM and c) AM.

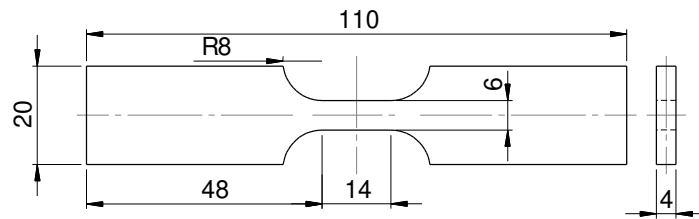


**Fig 2.** Smooth plane specimen geometry of X52 piping steel (X52\_SP).

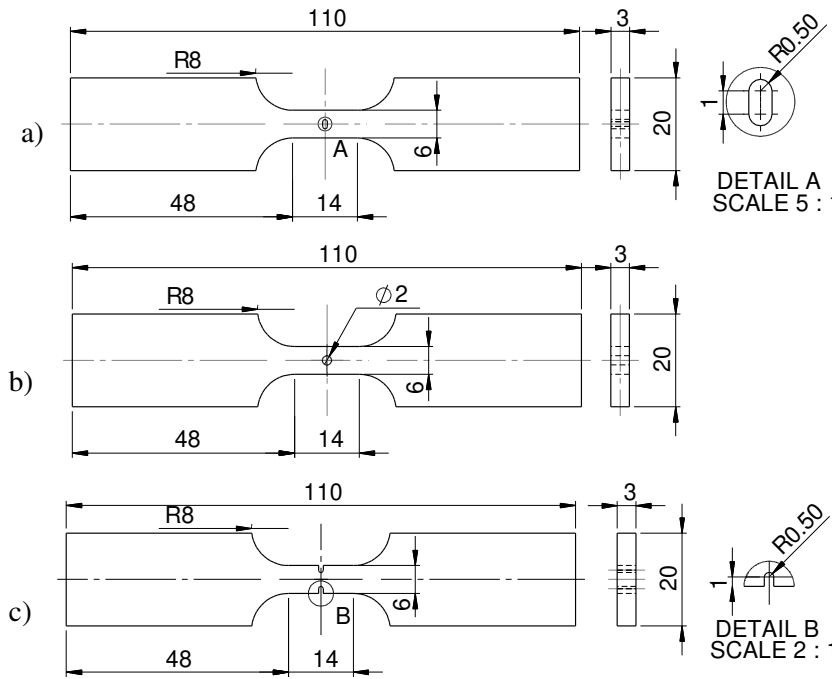


**Fig 3.** Notched plane specimens' geometries of X52 piping steel: a) central oval hole (X52\_OH); b) central circular hole (X52\_CH); c) double side notched (X52\_SN).

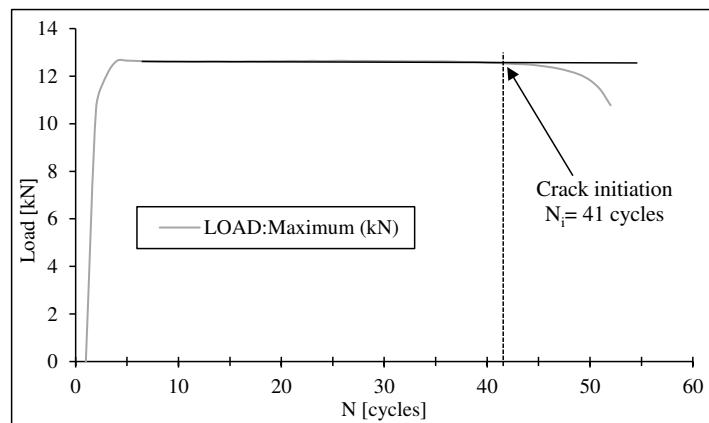


**Fig 4.** Criterion to assess the fatigue crack initiation (X52\_U0\_SP\_12).

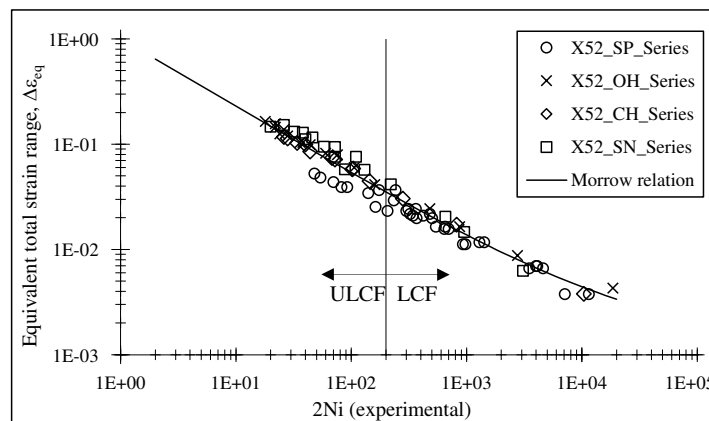


**Fig 5.** Total strain-life data of the X52 piping steel and correlation using Morrow relation with critical node approach.

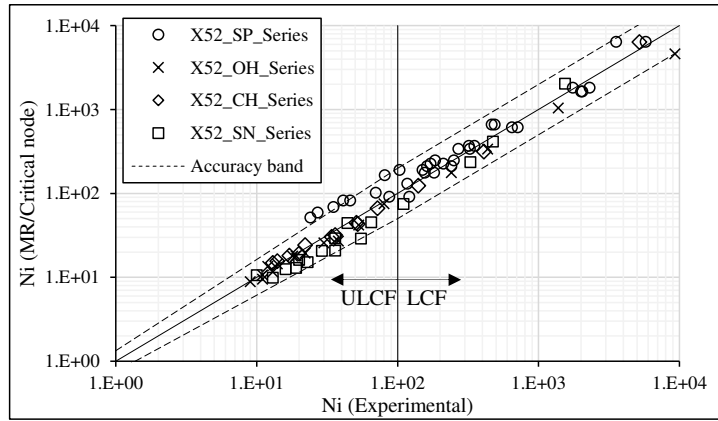


**Fig 6.** Comparison of experimental data and Morrow's predictions based on critical node approach predictions, for the X52 piping steel.

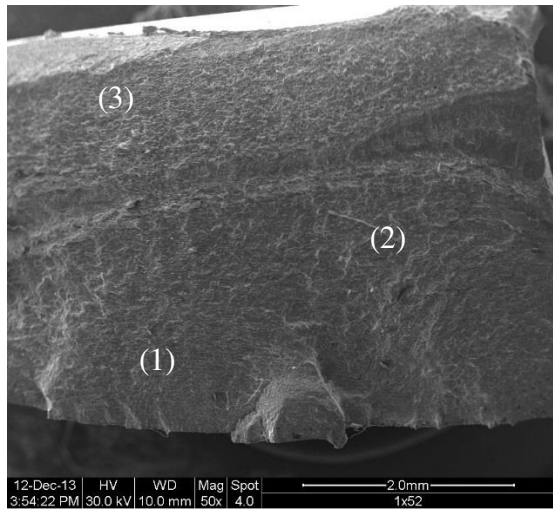


**Fig 7.** Fracture surface of smooth plane specimens of X52 piping steel, tested under ULCF domain ( $\Delta\varepsilon=5\%$ ).

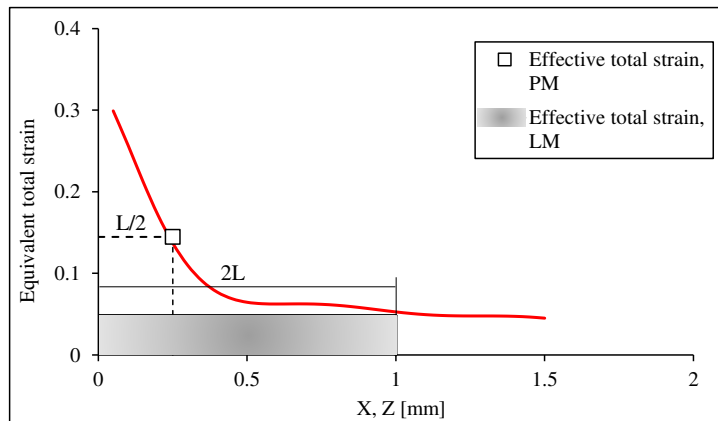


**Fig 8.** Equivalent total strain distribution along crack propagation direction of notched specimen (X52-U-1\_OH\_01).

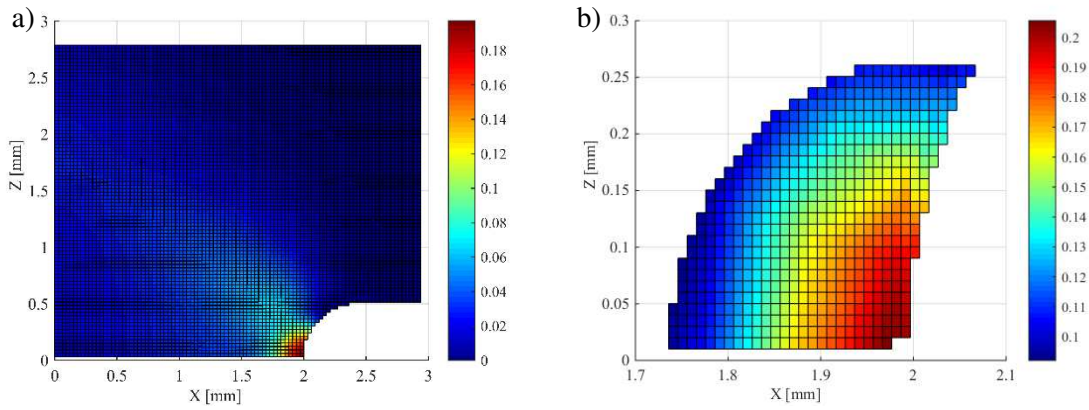


**Fig 9.** a) Illustration of the relevant effective equivalent total strain computation for the TCD using AM method (Z – loading direction); b) circular region considered to estimate effective equivalent total strain.

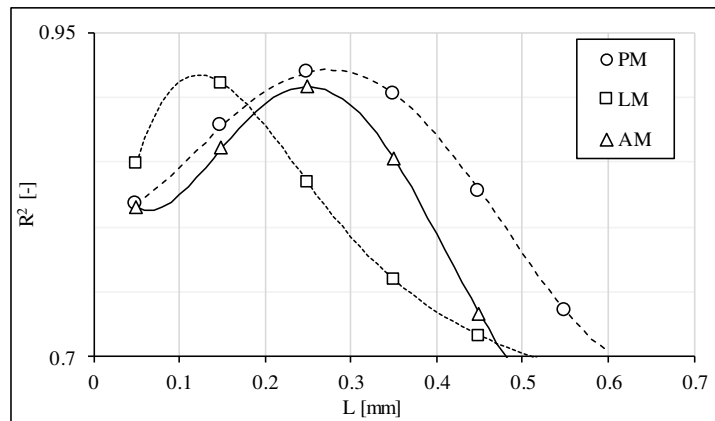


**Fig 10.** Determination coefficient  $R^2$  as function of critical distance,  $L$ .

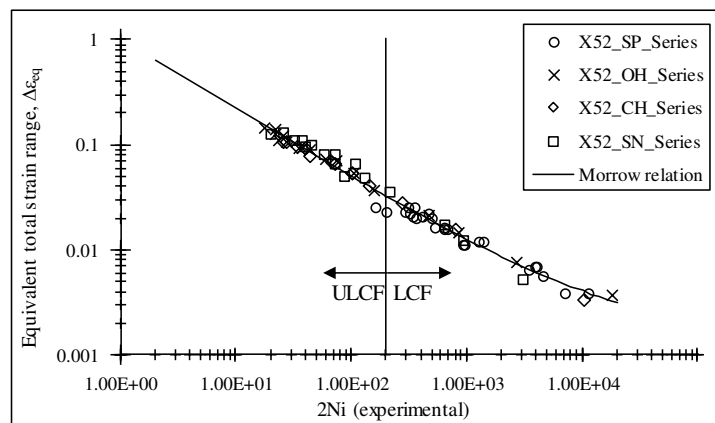


**Fig 11.** Correlation of the strain-life data obtained with the effective equivalent total strain computed using the TCD/PM ( $L=0.27$  mm).

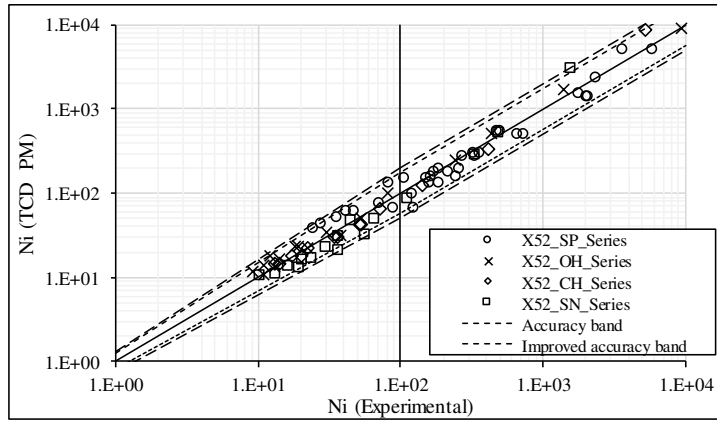


**Fig 12.** Comparison of experimental data and Morrow's predictions based on point method approach predictions, for the X52 piping steel.

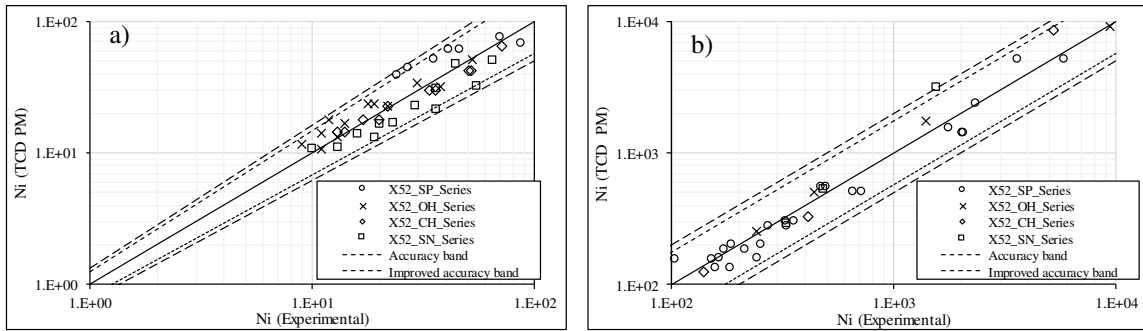


**Fig 13.** Comparison of experimental data and Morrow plus PM method for X52 piping steel under LCF (a) and ULCF (b) domains.

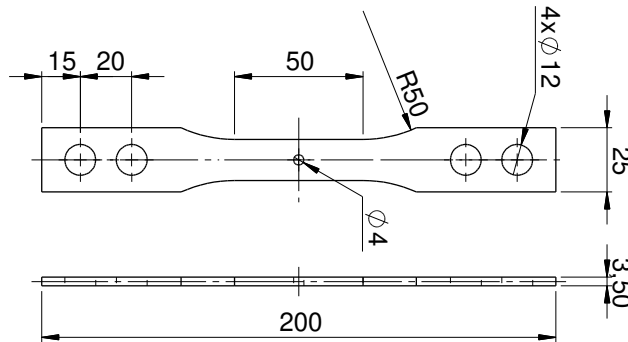


**Fig 14.** The geometry of plane notched specimen of X52 piping steel submitted to cyclic bending conditions (X52\_BNP).

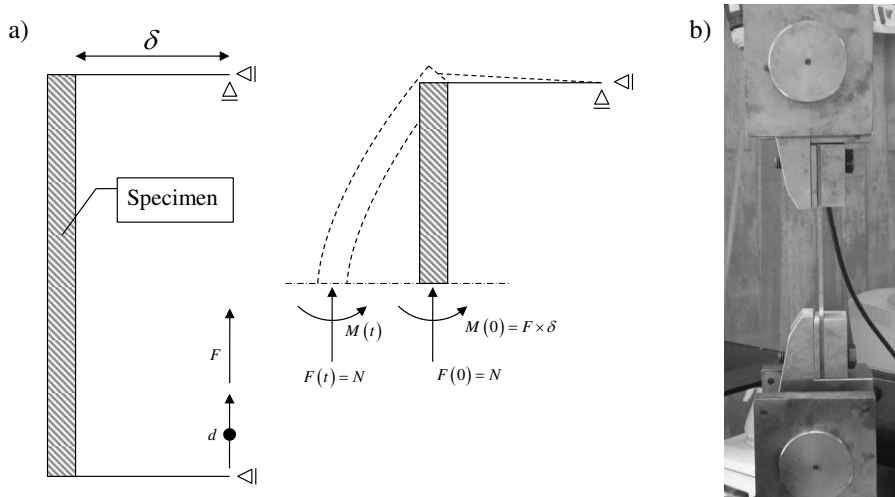


**Fig 15.** a) Loading conditions of the cyclic bending tests; b) grip system mounted in the test machine.

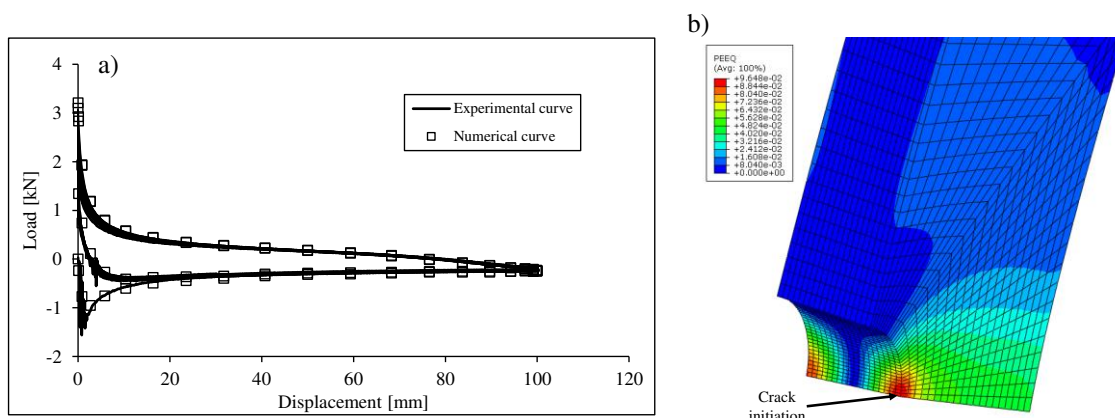


**Fig 16.** a) Numerical load-displacement curves correlated with experimental data (X52\_U\_BNP\_01); b) equivalent total strain field indicates the location for the crack initiation (X52\_U\_BNP\_13).

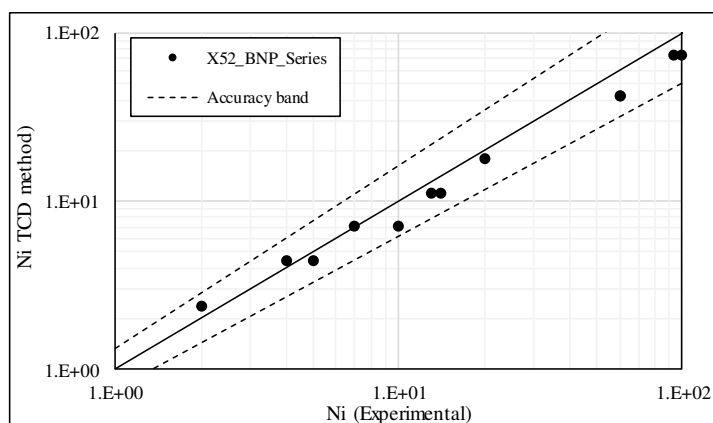


**Fig 17.** Prediction of the fatigue lives for the notched bending specimens made of X52 piping steel (X52\_BNP) using the TCD/PM with Morrow's equation.